ARCHIVE OF MECHANICAL ENGINEERING

DOI: 10.24425/ame.2024.151337 2024, Vol. 71, No. 4, pp. 561–580

Ahmed Tawfeeq Mustafa Ali ABED [1]

Computational analysis of SD7037 airfoil with plain flap

Received 18 July 2024, **Revised** 5 October 2024, **Accepted** 8 October 2024, **Published online** 31 October 2024

Keywords: aerodynamic characteristics, lift, drag, drag polar, UAV

The impact of a simple trailing-edge plain flap on the aerodynamics of the SD7037 airfoil have been studied in this paper using computational fluid dynamics at Reynolds number of 3×10^5 across various low angles of attack and flap deflection angles. The computational model was evaluated by using Star CCM+ software with κ–ω SST turbulence and gamma transition model to solve Navier-Stokes equations. The accuracy of the computational model has been confirmed through comparison with experimental data, showing a high level of agreement at low angles of attack. The findings revealed that specific combinations of angles of attack and flap deflection angles could increase the lift-to-drag ratio by over 70% compared to baseline conditions, benefiting airfoil performance, particularly during takeoff. Some combinations, however, resulted in decreased performance and should be avoided. The results also showed that with the increase of either the angle of attack or the flap deflection angle, the pitching moment increased.

Nomenclature

AoA	angle of attack, degree
c	airfoil chord, meters
cd	airfoil drag coefficient, dimensionless
CFD	computational fluid dynamics
cl	airfoil lift coefficient, dimensionless
cm	airfoil moment coefficient, dimensionless
cp	airfoil pressure coefficient, dimensionless
δ_f	flap deflection angle, degree

✉ Ahmed Tawfeeq Mustafa Ali ABED, e-mail: a.t.abed@coeng.uobaghdad.edu.iq

[1] Department of Aeronautical Engineering, College of Engineering, University of Baghdad, Baghdad, Iraq

1. Introduction

Flaps are developed and utilized to increase the lift of the aircraft, reduce stalls airspeed, and decrease takeoff and landing distances. They are also used in Unmanned Aerial Vehicles (UAV) to control lift, drag, and flight stabilization. They also optimize aerodynamics during takeoffs and landings. This improves maneuverability, stability, and efficiency of the UAVs, hence extending their radius of action. Therefore, they are very important for enhancing functionality across different applications. There have been variations of flaps configuration which were developed to achieve specific desired effects over time, as stated by Anderson [1] and Sadraey [2]. Plain flaps are not the best ones in terms of aerodynamic performance but they are easier to manufacture and apply in UAV, especially when it comes to the cost and reliability, as compared to the other types such as the slotted flap or the Fowler flap, Sadraey [2]. Then, studying the airfoils with plain flaps may benefit a wide range of UAV designers and manufactures, including amateurs.

The options for integrating two-element airfoils in the development of tactical UAVs were considered by S. Wang and G. Zheng [3]. The process of choosing an initial airfoil for segmentation, comparing different segmentation methods, and utilizing the NAGA-II algorithm to enhance aerodynamic efficiency by optimizing slot parameters were presented. Then, the enhanced airfoil was implemented on the Sparrow-hawk I UAV. They concluded a notable advancements in aerodynamic performance across various operational scenarios.

The performance of the NACA 23012 airfoil with plain flap for different variations of angle of attack from -5° to 20 and flap angle from -15° to 45° in low Reynolds number flow was measured experimentally and calculated computationally by N. Salam et al. [4]. The viscosity was computed using κ–ε turbulent model. The study revealed that the best lift-to-drag ratio occurred at 0° angle of attack and 15° flap angle.

Vimal Patel et al. [5] simulated the M21 airfoil with various flap designs for different angles of attack (AoA) to determine the maximum lift force and stall angle using computational fluid dynamics (CFD) analysis. The work included simulation of a plain flap. It was concluded that the stall angle reached for M21 was 24° and the maximum value of lift-to-drag ratio measured at 7° AoA. The investigation also showed that for the 10° plain flap angle, the highest drag and lift force was possible.

The effect of the flap's deflection angle on flow characteristics in NACA 4415 airfoil using XFoil software, in inviscid conditions, were analyzed by G.A. Vinod and T.J.S. Jothi [6]. It was concluded that for flap angles above 0°, the airfoil can produce an abrupt increase in lift which is useful in takeoff conditions. While the flap angles are set below zero degrees, the lift is observed to decrease contributing to a greater drag.

G. Ramanan et al. [7] calculated the aerodynamic characteristics of SD7037 airfoil at a low Reynolds number for a fixed wing UAV using CFD. Model design

considerations for the SD7037 low Reynolds number airfoil have been used to design and analyze the UAV. The aerodynamic induced drag factor of the aircraft was chosen as a parameter for the design method and was approximately calculated for the airfoil and wing characteristic curves. The calculated aerodynamic data were successfully utilized as the input for self-stabilizing the UAV in various test conditions.

The effects of plain flap over the aerodynamic characteristics of NACA 66-015 airfoil was thoroughly investigated by I. Singh [8], both experimentally and numerically. No considerations for the viscosity effects were mentioned. The analysis revealed that the use of flap enhanced the performance of the airfoil at different angles of attack, and the results of the numerical model agreed well with the experimental measurements. The airfoil reached the maximum lift coefficient AoA 9°. Stall occurred above that angle and the airfoil was fully stalled at 15°.

Pracheta et al. [9] utilized CFD to study the flow around NACA 2412 airfoil with flap at different Reynolds numbers ranging from 3.2×10^5 to 12.4×10^5 with different AoA values and deflection angles configurations. It was concluded that application of flaps resulted in increased lift coefficients. However, it was discovered that at higher values of AoA, the lift coefficient decreased as a result of a decrease in the stall angle. It is worth to mention that the study did not simulate the boundary layer due to the lack of computational power.

The analysis of the aerodynamic properties of an airfoil with different types of flaps aimed at designing an effective wing for UAV aircraft at low Reynolds numbers was carried out by S. Srivastava and C.V.N. Aditya [10]. The CFD was applied via Ansys software on a two dimensional model without the inclusion of any inflation layers, and without considerations for the boundary layer, which affected the reliability of results of the drag. The research concluded that the maximum increase in lift coefficient occurred at 10° flap deflection when using a single slotted flap. It is worth to mention that the paper didn't take into consideration the complexity of such a flap system, especially for a UAV!

Lift characteristics may be studied theoretically to a high degree of accuracy without any considerations for the flow viscosity, however, the same is not true for the characteristics of the drag. Studying drag characteristics needs not only to simulate the viscosity, but also to model accurately its behavior and effects. This can be done based on the Reynolds number using various viscous models, Anderson [1].

Different turbulence models for the flow over various types of airfoils at low Reynolds numbers were created by researchers to study the aerodynamics of airfoils. From their work, one can conclude that the use of κ–ω SST with the gamma transition model makes it possible to provide accurate predictions for lift and drag coefficients [11–15].

Most of the recent and previous studies did not conduct any thorough study on the use of SD7037 airfoil with flap for UAVs. This airfoil provides a remarkable

efficiency when high endurance is concerned, however, it suffers from performance degradation at low Reynolds numbers, as stated in M.S. Selig et al. [16].

The objective of this work is to study the aerodynamic characteristics of the SD7037 airfoil with added trailing edge flap at low angles of attack by solving the Navier–Stocks equations using CFD tools with κ–ω SST turbulence and gamma transition model provided by Siemens Star CCM+ software package.

2. Computational model and setup

2.1. The model

In this work, an airfoil with SD7037 profile was chosen, and a chord length of 0.23 m was assumed as a typical value for the purpose of this research. A simple plain flap at the trailing edge was added to the airfoil at the 0.79% chord location, making the flap chord 21% of the total chord of the airfoil. The flow conditions were set up at the sea level. The value chosen for the free stream Reynolds number was 3×10^5.

These values were chosen to compare the numerical calculations with the experimental measurements available from M.S. Selig et al. [16]. It should be noted that the experimental data is only available for the clean airfoil and for the airfoil with a plain flap at deflection angles (δ_f) of 0°, 5°, and 10°.

The geometrical data for the airfoil were taken from M.S. Selig et al. cite16 and the modeled using CAD tools available in the Siemens Star CCM+ software package, as shown in Fig. 1.

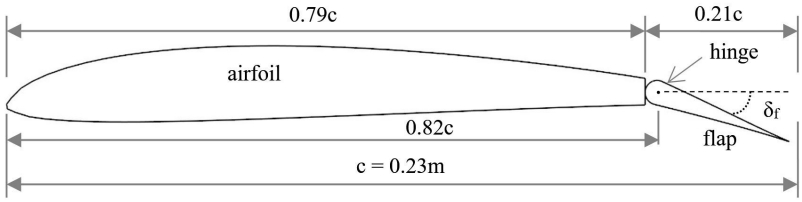

Fig. 1. Airfoil and plain flap geometry

The flap has been modeled with the hinge point, the point around which the flap deflection angle is measured, located at 0.82c from the wing leading edge, or 0.3c from the flap leading edge.

2.2. Computational setup

The airfoil was simulated for two dimensional steady-state incompressible viscous flow conditions. In these conditions, the flow over the airfoil was expected to be mixed laminar-turbulent, as the local Reynolds number may reach and exceed the value of 5×10^5, thus Reynolds-Averaged Navier–Stokes (RANS) equations

were utilized to compute the viscosity effects. Specifically, and in order to simulate the transition from laminar to turbulent conditions, κ–ω SST turbulent model introduced by F.R. Menter [17] with gamma transition was chosen. This meant that the value of y+ must be unity or less over the airfoil to ensure reliable results, as mentioned by H.K. Versteeg and W. Malalasekera [18]. It has been also taken into considerations that the vortices generated in the airfoil-flap connection region require the simulation of turbulent flow rather than only laminar.

The computational domain was selected to be a square of 20 meters to ensure no interaction between the boundaries of the domain and the airfoil. The inlet was set to be the velocity inlet, and the pressure outlet was set on the domain exit, as shown in Fig. 2.

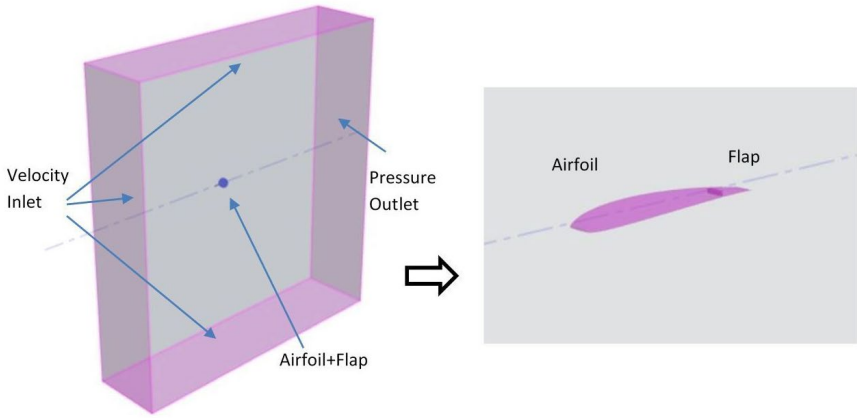

Fig. 2. Two dimensional computational domain, airfoil with flap and boundary conditions

The use of an unstructured mesh was chosen to discretize the flow domain due to its flexibility, as presented by H.K. Versteeg and W. Malalasekera [18]. The current work deals with a complex flow near the flap, as shown in Fig. 1 above.

It is expected that due to sudden changes of flow from the airfoil surfaces to the flap surfaces, vortices appear in the flow near the leading edge of the flap. This effect will become more obvious at higher AoA and δ_f. The mesh over the airfoil and the flap was structured so as to capture flow characteristics in detail and ensure reliable and accurate results. Thus, polygonal cell type was used due to its high quality, accuracy, and stability, although it requires a higher computational power.

The boundary layer over the airfoil and the flap was taken into account, using typical values of 20 prism layers near the airfoil and flap walls, with the thickness of the first layer equal to 2.12×10^{-5} m calculated using the method presented by H.K. Versteeg and W. Malalasekera [18].

The flow characteristics mostly change near the airfoil and the flap, so the cells were concentrated around the whole airfoil, with another refinement layer added around the flap to capture the flow changes.

The wake, which is crucial for determining aerodynamic characteristics, was modeled to be 20 times longer than the length of the airfoil in the trailing edge direction.

These settings were refined through a mesh independence study to ensure accuracy of the solution. The final mesh is presented in Fig. 3.

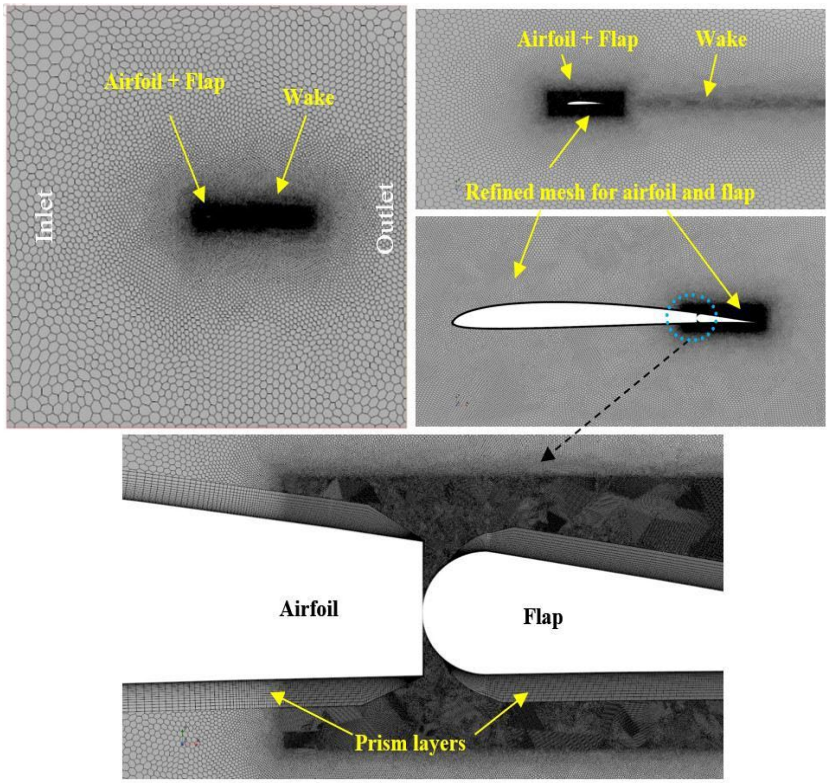

Fig. 3. Meshing of the model

The mesh independence study, shown in Fig. 4 below, has shown that the computational solution becomes stable around 649,546 cells. In order to reduce the computational power and time required for the analysis, while maintaining an acceptable level of accuracy, the number of cells used for this research is then chosen equal to 469,303, as the difference between the values of the lift coefficient between these two cases is only 0.2%.

3. Validation

To ensure the correct application of CFD principles, recommendations, and properly use the tools provided by the software package, a verification is necessary. M.S. Selig et al. [16] provided experimental data for the SD7037 airfoil with a flap.

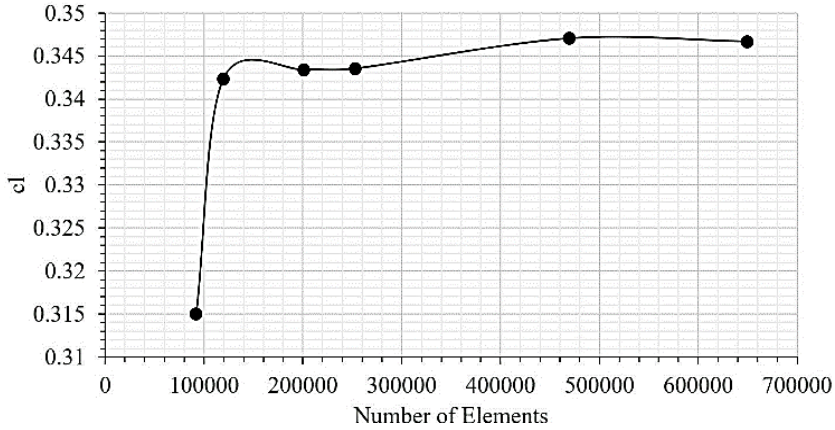

Fig. 4. Mesh independence study

These data include flap deflection angles of 0°, 5°, and 10° at various Reynolds numbers, which will be used for the verification case.

The computational setup described in the previous section was applied to the angle of attack (AoA) range from 0° to 6° and flap deflection angles δ_f of 0°, 5°, and 10°.

The computational results show good agreement with the experimental measurements from M.S. Selig et al. [16] for the investigated cases, as demonstrated in Fig. 5 below. Based on the computational model, the lift coefficient was accurately calculated for the three cases of different flap deflection angles and for various angles of attack up to 6°.

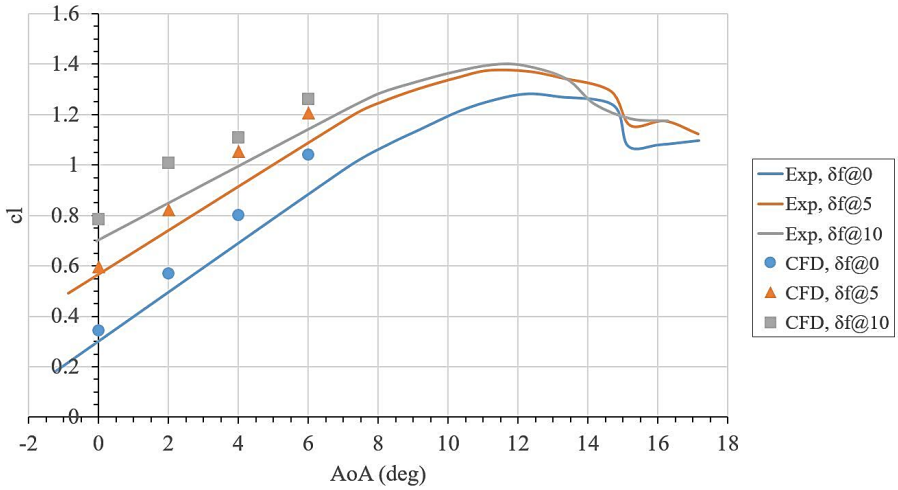

Fig. 5. Comparison of cl between experimental data and CFD model at various AoA

The drag polar was also analyzed, as shown in Fig. 6, from which it could be deduced that the proposed model may simulate the flow conditions assumed in the current work at low AoA with an acceptable accuracy.

It can be seen that using the methods proposed in the current work one can compute the aerodynamics characteristics accurately up to AoA 6°, which well serves the purpose of this paper.

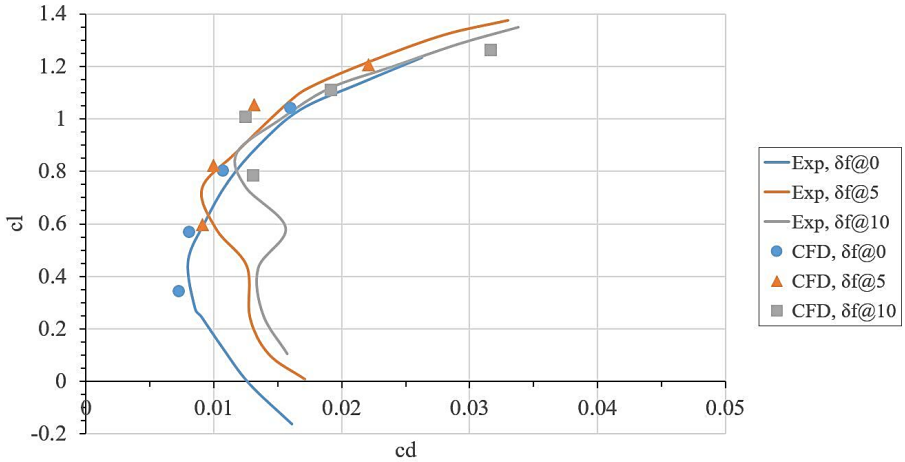

Fig. 6. Comparison of drag polar between experimental data and CFD model

4. Results

In this section, the aerodynamic characteristics of SD7037 airfoil with plain trailing edge flap are computationally determined for the range of AoA from 0° to 6° and the flap deflection angle δ_f of 0°, 5°, 10°, 15°, and 20° at sea level conditions with free stream Reynolds number value of 3×10^5. The values for AoA, δ_f, and the Reynolds number represents the practical range of operation for a high aspect ratio wings and flaps in UAVs during takeoff and landing phases.

4.1. Lift coefficient

Fig. 7 illustrates the lift coefficient (cl) versus the angle of attack (AoA) for various values of δ_f. The computational analysis from this study is labeled as CFD and represented on the chart with either symbols only or solid lines with symbols. The data show that the lift coefficient increases with higher AoA for a given δ_f, and also increases with higher δ_f for a given AoA.

The lowest cl value occurs at AoA 0° and δ_f 0°, while the highest cl value is seen at AoA 6° and δ_f 20°.

Fig. 8 shows a graph of cl versus δ_f for different AoA, from which the same conclusions can be drawn, also it can be seen that the gain in cl from δ_f 10° is lower

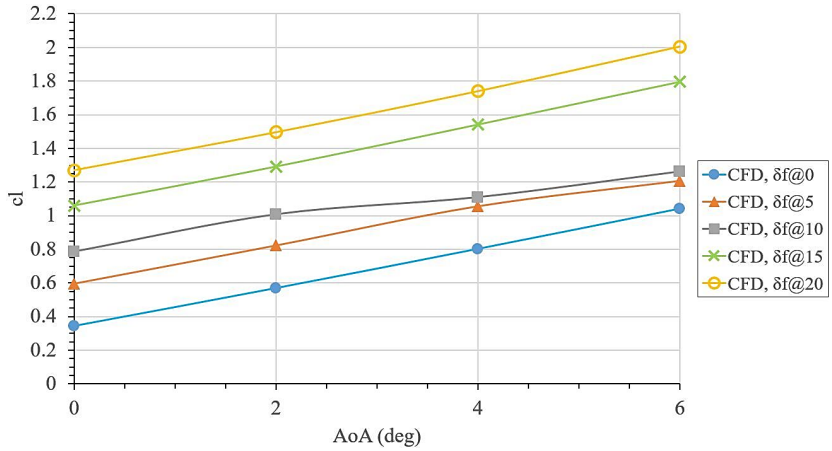

Fig. 7. Lift coefficient versus angle of attack for different flap deflection angles

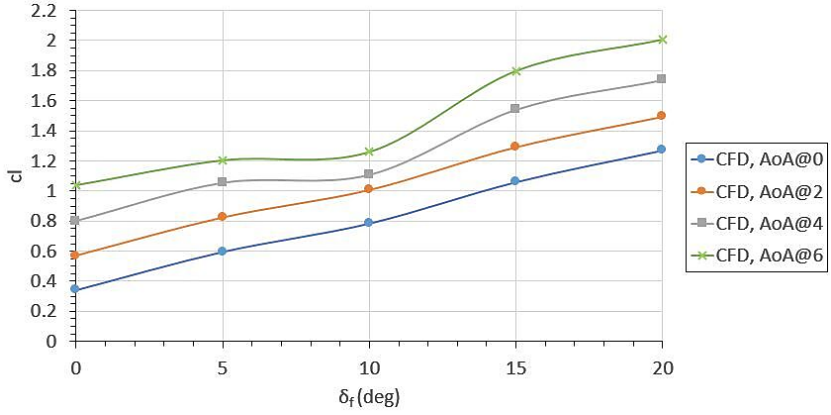

Fig. 8. Lift coefficient versus flap deflection angle for different angles of attack

than in other cases and this gain decreases as AoA increases. A smaller increase was noticed at δ_f 10° and AoA 6°.

The analysis of pressure coefficient cp contours at 6° AoA for δ_f of 5°, 10°, and 15°, illustrated in Fig. 9 below, reveals that altering the flap angle impacts the pressure distribution on the airfoil. This adjustment influences the suction peak on the upper surface and the positive pressure on the lower surface in two ways. Firstly, it increases the magnitude of these peaks, and secondly, it expands the region over which these peak values are sustained by the airflow.

Comparing the cases of flap deflections δ_f at 5° and 10°, makes it evident that the area affected by the pressure peaks is reduced and the difference between the two peak values is smaller for the 10° deflection, as observed in Fig. 8. This phenomenon also occurs at a 4° AoA for the flap deflection δ_f of 10°.

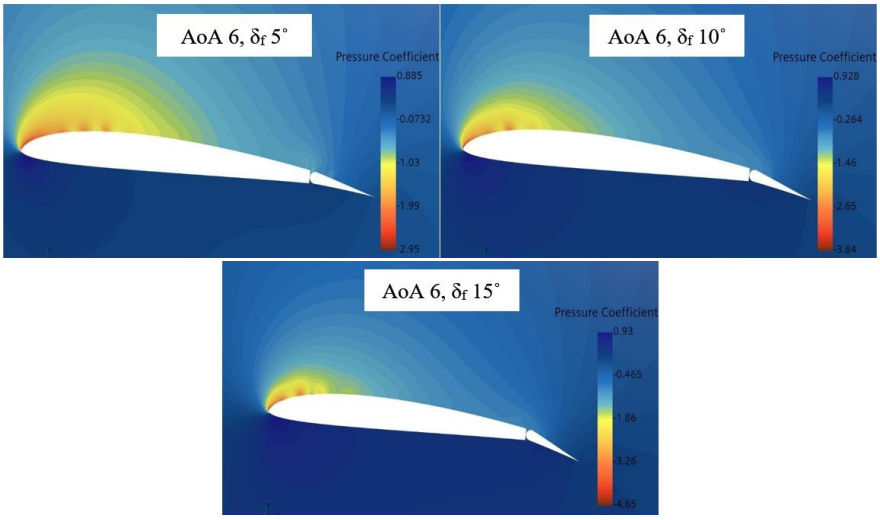

Fig. 9. Contours of pressure coefficient at AoA 6° for different flap deflection angles

4.2. Drag coefficient

The drag coefficient (cd) versus the angle of attack (AoA) for various values of δ_f is shown in Fig. 10. The data show that the drag coefficient increases with higher AoA for a given δ_f, and also increases with higher δ_f for a given AoA. The lowest cd value occurs at AoA 0° and δ_f 0°, while the highest cd value is seen at AoA 6° and δ_f 20°. There were no signs of flow separation.

Fig. 11 shows cd versus δ_f for different AoA, from which the same conclusions can be drawn, also it can be seen that at AoA 0°and δ_f 10° there is an increase of cd which exceeds that of AoA 2°and δ_f 10°. Examination of pressure coefficient

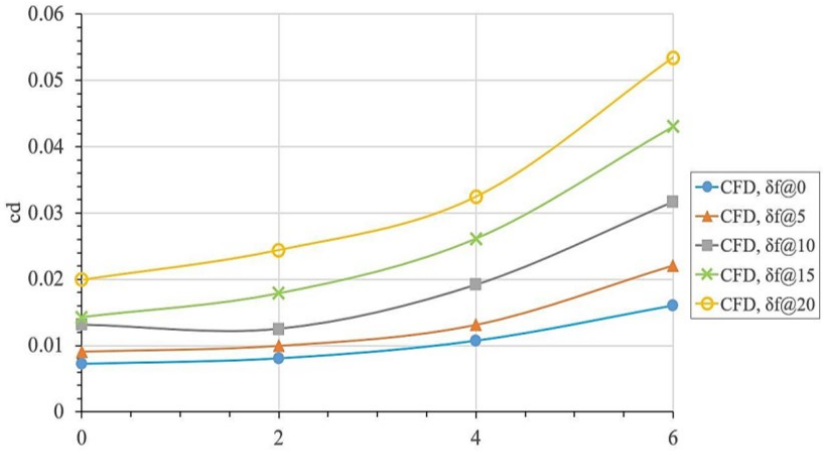

Fig. 10. Drag coefficient versus angle of attack for different flap deflection angles

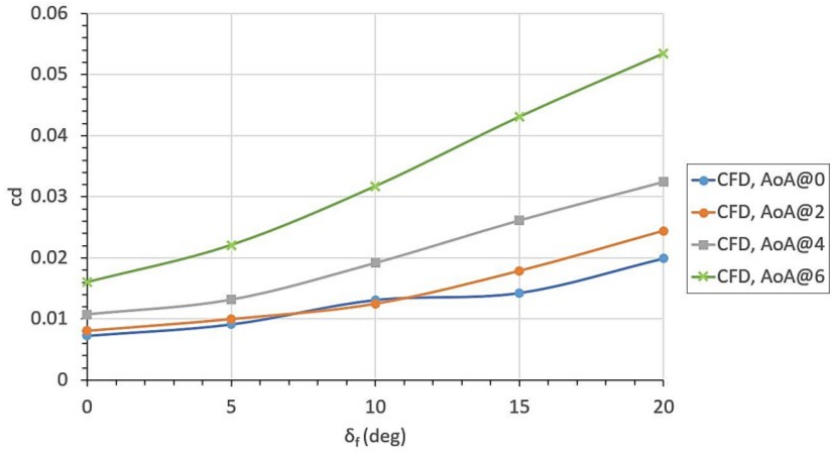

Fig. 11. Drag coefficient versus flap deflection angle for different angles of attack

contours in Fig. 12 show that in the case of AoA 0°and δ_f 10° the flow exhibits stronger vortices, and a loss of energy on the lower surface near the flap hinge point, which results in an increase of drag, as compared to the case of AoA 2°and δ_f 10°.

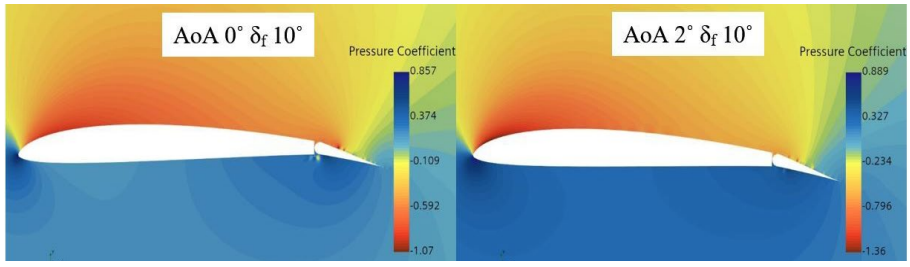

Fig. 12. Contours of pressure coefficient at AoA 0° δ_f 10° and AoA 2° δ_f 10°

4.3. Lift to drag ratio

The analysis of lift coefficient is not sufficient to decide if the addition of the flap would enhance the performance of the airfoil and at which deflection angle the airfoil would optimally perform. The performance is measured by the lift produced, the gain, the drag generated, the cost, or cl to cd ratio (cl/cd).

Fig. 13 shows the lift to drag ratio drawn versus AoA. It can be concluded that the best performance (the highest cl/cd) occurs at AoA 2°, and δ_f 5°. The second best performance occurs at AoA 2°, and δ_f 10° with the cl/cd value very close to that of the third option, where AoA 4°, and δ_f 5°. While, the worst performance is observed at AoA 6°, δ_f 20°, when the airfoil produces the highest lift and the highest drag with the lowest lift to drag ratio.

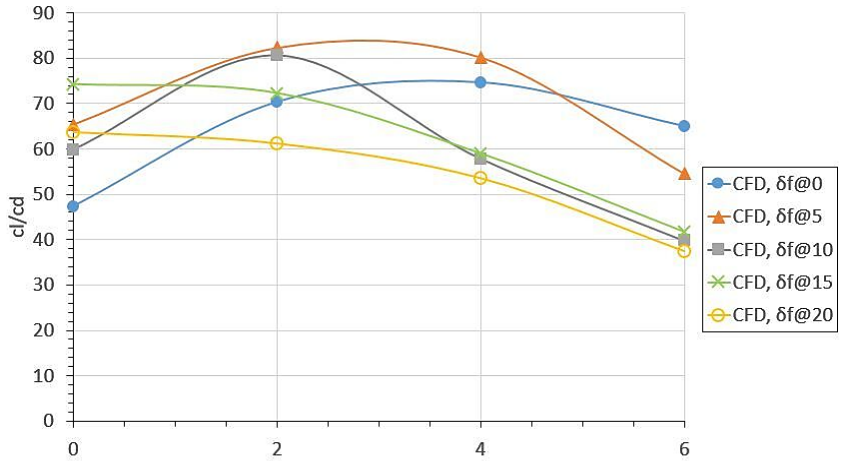

Fig. 13. Lift to drag ratio of airfoil and flap at various angles of attack and flap deflection angles

The percentage changes in the values of cl, cd, and cl/cd compared to the base case where AoA 0°, δ_f 0° are shown in Table 1 in Appendix where the results are sorted from the best to the worst value of lift to drag ratio.

These results can be practically applied to determine the optimal UAV wing setup for the takeoff phase. It can also be noted that the drag values increase with the increase of the deflection angle even at 10° and a low AoA, which is due to the geometry in the airfoil-flap area. The analysis of velocity distribution in the model can help explaining the results shown in Table 1 in Appendix.

Figs. 14–17 show the velocity magnitude and vorticity contours (scaled by Log10) side by side at AoA 0°, δ_f 0°, AoA 2°, δ_f 5°, AoA 2°, δ_f 10°, and AoA 6°, δ_f 20°, respectively. The flow approaches the model at a zero angle of attack and meets the airfoil at the leading edge, comes to a full stop before accelerating on the upper and lower surfaces, and reaches its maximum velocity of about 24 m/s approximately 0.25c from the leading edge at the upper surface, as shown in Fig. 14.

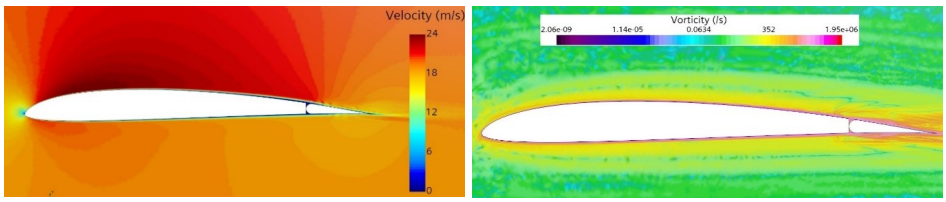

(a) (b)

Fig. 14. Velocity distribution (a) and vorticity scaled by Log10 (b) at AoA 0°, δ_f 0°

Near the walls, the flow slows down until it reaches zero height from the wall, due to the no-slip condition. As the flow approaches the airfoil-flap area and due

to sudden changes in its direction, vortices start to form and some of them travel along the flap towards its trailing edge, as show in Fig. 14b. The size and strength of these vortices affects both lift and drag, hence, the effectiveness of the flap. These vortices are directly affected by the angle of attack and the flap deflection angle.

It can be seen that, in the case AoA 2°, δ_f 5°, the velocity difference between the upper and lower surfaces is higher, hence the pressure difference is higher, as shown in Fig. 15.

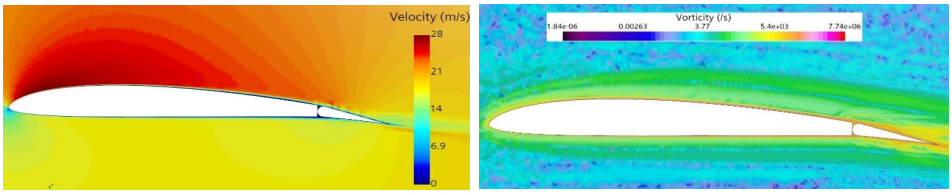

(a) (b)

Fig. 15. Velocity distribution (a) and vorticity scaled by Log10 (b) at AoA 2°, δ_f 5°

This difference results in a higher lift coefficient, and the vortices generated in airfoil-flap area are small and moving towards the trailing edge without increasing in strength or size, thus the drag is not significantly increasing, compared to the base case. The same behavior can be seen in Fig. 16 at AoA 2°, δ_f 10°.

At AoA 6°, δ_f 20° the flow is affected by separation near the leading edge, as shown in Fig. 17. Although the flow is contained and small, it causes loss of energy along the upper surface of the model resulting in large vortices near the flap, which very significantly increases the drag. A further increase in drag is generated in the airfoil-flap area due to the loss of energy and the pressure drop that leads to a pressure difference in the chord-wise direction (x-axis), i.e., the pressure drag.

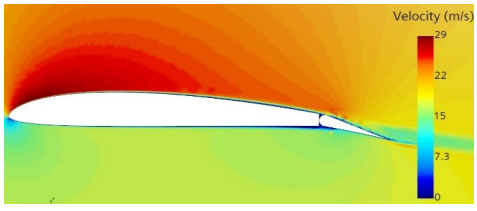

Fig. 16. Velocity distribution at AoA 2°, δ_f 10°

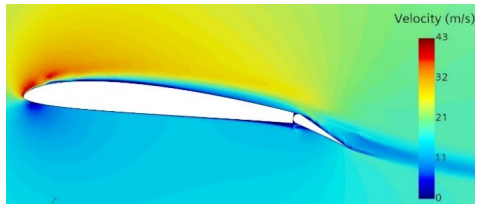

Fig. 17. Velocity distribution at AoA 6°, δ_f 20°

4.4. Moment coefficient

Fig. 18a shows the moment coefficient (cm) versus AoA at δ_f, which is taken around the airfoil's leading edge. Note that the negative value of cm denotes its counterclockwise direction, the moment that tends to restor the airfoil to its original state of equilibrium. In this case it is acting around the leading edge in counter

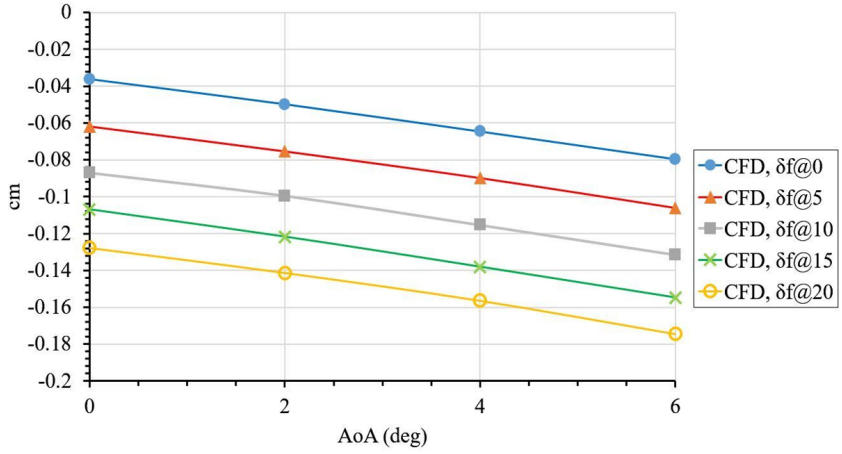

(a)

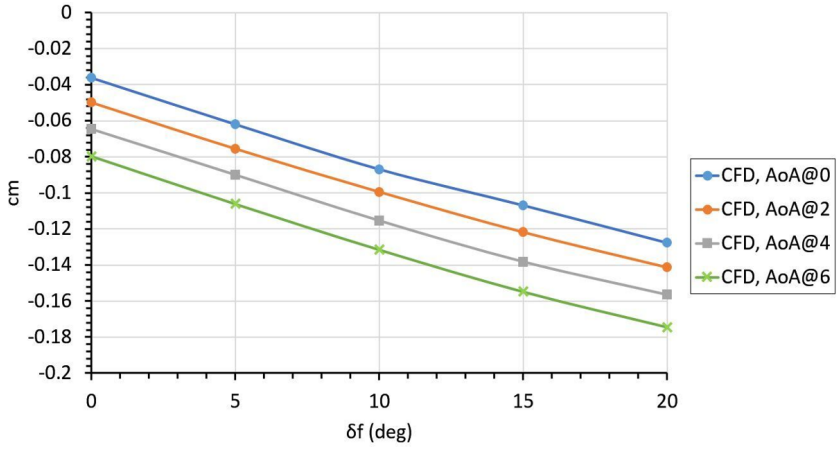

(b)

Fig. 18. Moment coefficient versus angle of attack (a) and flap deflection angles (b)

clockwise direction. One can conclude that as AoA increases, the pitching moment increases, which is due to the increased net aerodynamic forces on the upper surface of the model. The same behavior can be seen in Fig. 18b, as the moment increases with the increase of δ_f for different AoAs. This means that during the takeoff the increased δ_f causes that the airfoil will pitch down to balance the moment.

4.5. Pressure distribution

Examination of pressure distribution over the airfoil and flap surfaces is necessary to understand the flow behavior in different conditions.

Fig. 19 shows the pressure distribution in terms of pressure coefficient at AoA 0° for different flap deflection angles. It can be seen that due to the shape of the

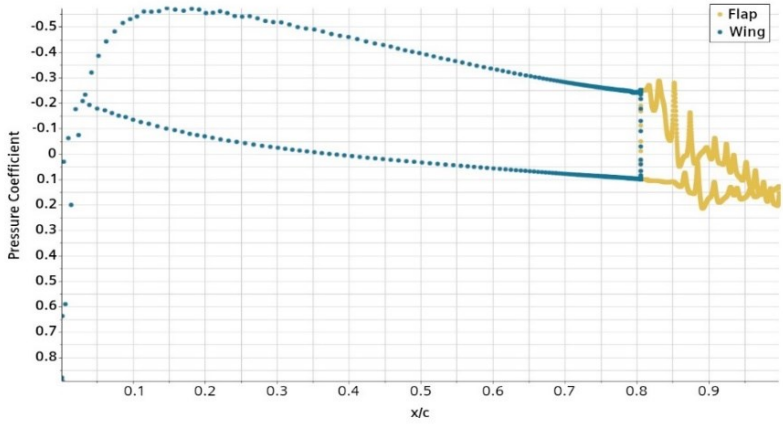

(a) δ_f 0°

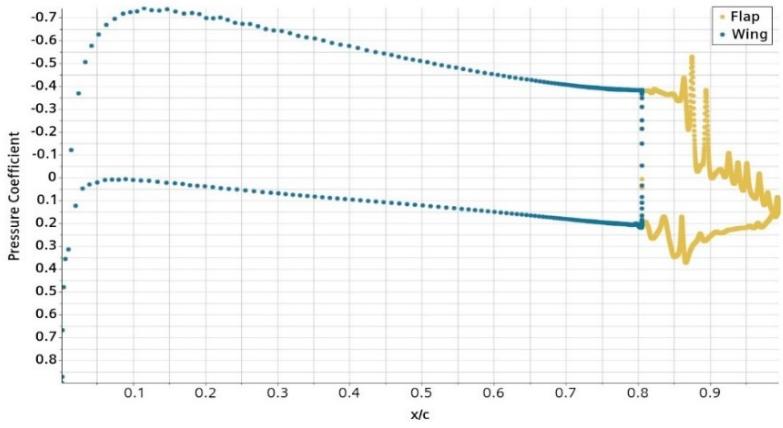

(b) δ_f 5°

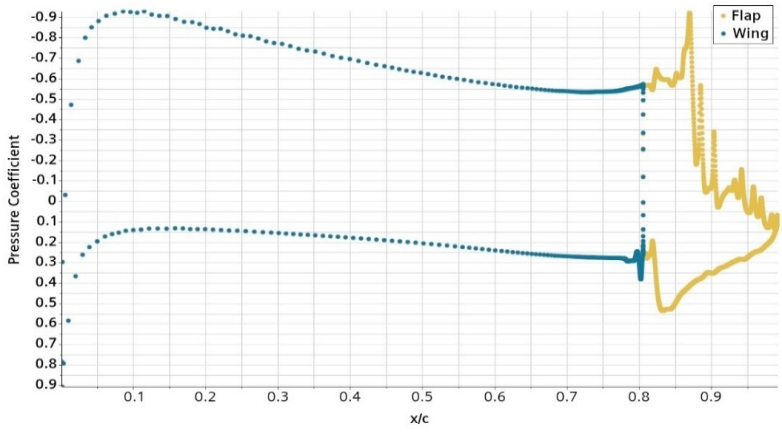

(c) δ_f 10°

Fig. 19. Pressure coefficient distribution at AoA 0° and various δ_f

junction area between the airfoil and the flap there appear turbulences and vortices generated in the flow, which cause a fluctuation in pressure along the chord of the flap. This behavior, in some cases, extends upstream the airfoil, as shown in Fig. 19e at δ_f 20°.

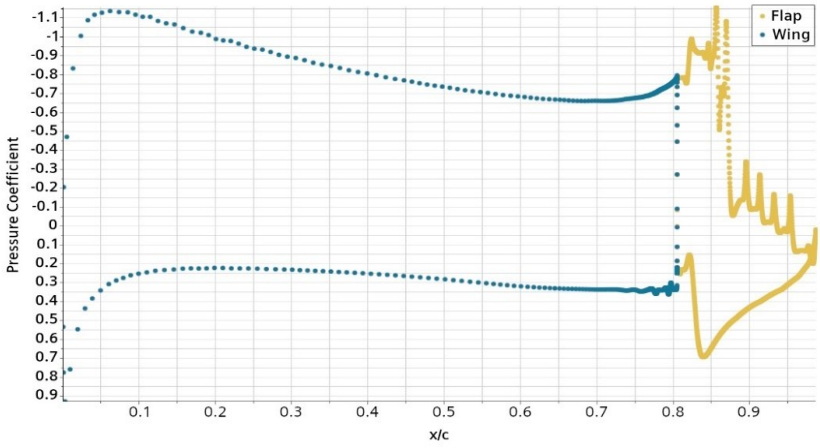

(d) δ_f 15°

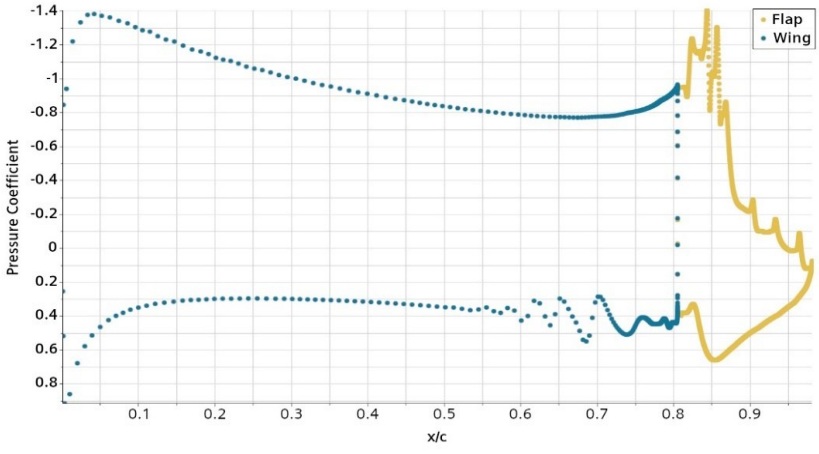

(e) δ_f 20°

Fig. 19. cont. Pressure coefficient distribution at AoA 0°, and various δ_f

According to Fig. 20, the same conclusion can be drawn for the distribution of pressure over the airfoil and the flap at AoA 2°, except that the effect of the turbulence in the junction area becomes stronger and more extended over the airfoil.

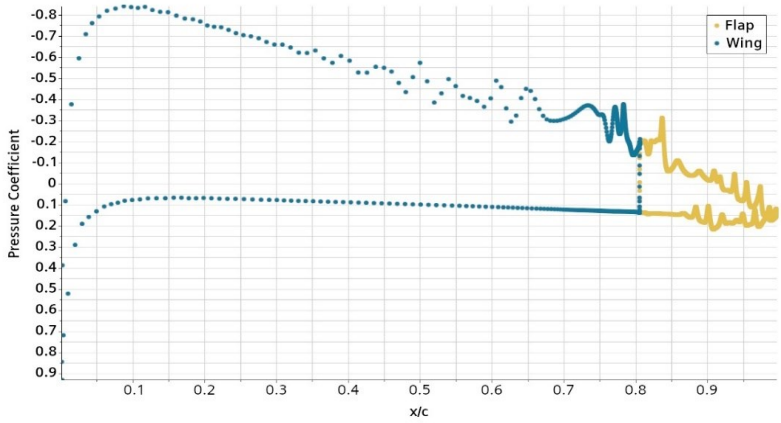

(a) δ_f 2°

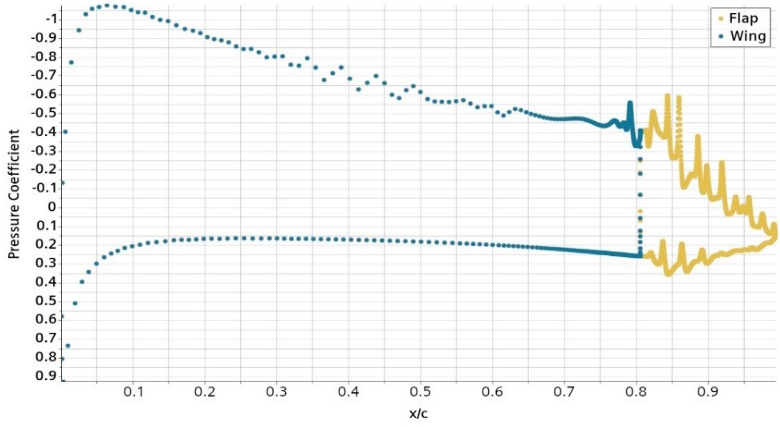

(b) δ_f 5°

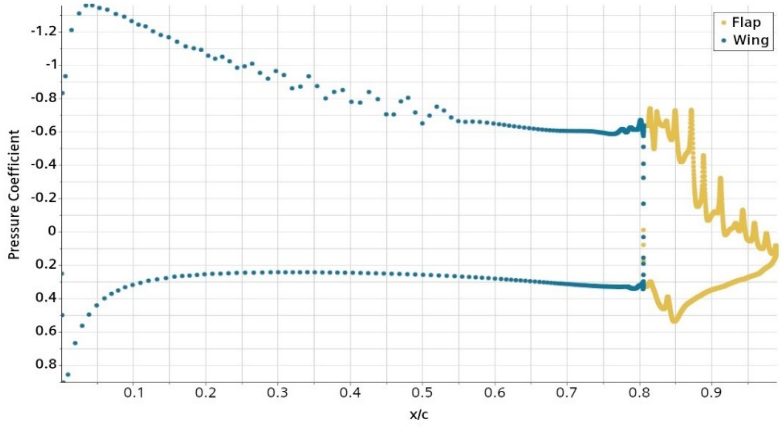

(c) δ_f 10°

Fig. 20. Pressure coefficient distribution at AoA 0° and various δ_f

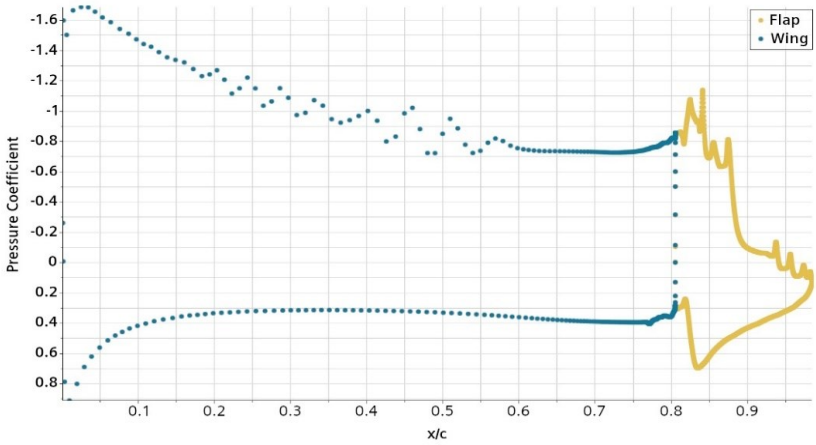

(d) δ_f 15°

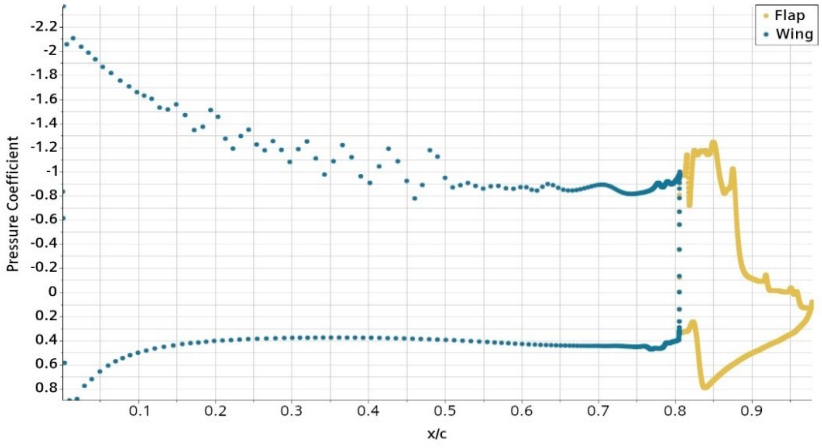

(e) δ_f 20°

Fig. 20. cont. Pressure coefficient distribution AoA 2° and various δ_f

5. Conclusions

This research delves into the aerodynamic properties of the SD7037 airfoil with trailing edge plain flap at low angles of attack and a low Reynolds number through CFD simulation conducted with the Siemens Star CCM+ software package. The study yielded the following conclusions:

1. It has been proven that using the turbulent model κ–ω SST with gamma transition to simulate the complex nature of the flow and capture the laminar – turbulent phenomena at low angles of attack yields good results, consistent with the available experimental measurements.

2. Although the design and construction of the plain flap is simple, it can generate high drag values at flap deflection angles higher than 10°, which is due to the flow turbulence in the airfoil-flap region.
3. The best lift to drag ratio occurs at AoA 2°, δ_f 5°.
4. The worst lift to drag ratio happens at AoA 6°, δ_f 20°.
5. The pitching moment increases with the increase of either the angle of attack or the flap deflection angles.
6. Further research is required to investigate application of other types of flaps and explore their effects on airfoil characteristics and performance.
7. An experimental setup is required to extend the analysis of this paper for different Reynolds numbers and different types of flaps.

Appendix

The calculated aerodynamic characteristics of SD7037 airfoil with plain trailing edge flap for the range of AoA from 0° to 6° and flap deflection angle δ_f of 0°, 5°, 10°, 15°, and 20° at sea level conditions with free stream Reynolds number value of 3×10^5 are presented in Table 1.

Table 1. Lift to drag ratio of the airfoil and flap at various angles of attack and flap deflection angles as compared to base case AoA 0°, δ_f 0°

Case	AoA (deg)	δ_f (deg)	cd	cl	cl/cd
1	2	5	137.72%	239.82%	174.14%
2	2	10	172.17%	293.33%	170.37%
3	4	5	181.18%	307.49%	169.71%
4	4	0	147.90%	233.65%	157.98%
5	0	15	196.60%	308.72%	157.03%
6	2	15	246.21%	376.46%	152.90%
7	2	0	111.34%	165.67%	148.79%
8	0	5	125.72%	173.88%	138.31%
9	6	0	220.57%	303.39%	137.55%
10	0	20	274.45%	370.02%	134.83%
11	2	20	336.34%	435.76%	129.56%
12	0	10	180.75%	228.73%	126.54%
13	4	15	360.09%	449.36%	124.79%
14	4	10	264.01%	322.99%	122.34%
15	6	5	304.29%	351.38%	115.47%
16	4	20	446.97%	506.80%	113.39%
17*	0	0	100.00%	100.00%	100.00%
18	6	15	593.29%	523.67%	88.27%
19	6	10	436.79%	367.49%	84.14%
20	6	20	735.92%	584.06%	79.36%

*Reference configuration AoA 0°, δ_f 0°

References

[1] J.D. Anderson Jr. *Introduction to Flight*, 8th edition, McGraw-Hill Education, 2016.

[2] M.H. Sadraey. *Design of Unmanned Aerial Systems*, 1st edition, John Wiley & Sons Ltd, 2020. doi: 10.1002/9781119508618.

[3] S. Wang and G. Zheng. Design, optimization and application of two-element airfoils for tactical UAV. *Advances in Mechanical Engineering*, 14(11), 2022. doi: 10.1177/16878132221137027.

[4] N. Salam, R. Tarakka, Jalaluddin, D. Iriansyah, and M. Ihsan. The effects of flap angles on the aerodynamic performances of a homebuilt aircraft wing model. *International Journal of Mechanical Engineering and Robotics Research*, 11(12):908–914, 2022. doi: 10.18178/ijmerr.11.12.908-914.

[5] V. Patel, V. Rathod, and C. Patel. Numerical investigation of M21 aerofoil and effect of plain flapper at various angle of attack. *Journal of Physics: Conference Series*, 2070:012153, 2021. doi: 10.1088/1742-6596/2070/1/012153.

[6] G.A. Vinod and T.J.S. Jothi. Effect of flap deflection angle on flow characteristics of aerofoil. *IOP Conference Series: Materials Science and Engineering*, 1189:012039, 2021. doi: 10.1088/1757-899X/1189/1/012039.

[7] G. Ramanan, P. Radha Krishnan, H.M. Ranjan. An aerodynamic performance study and analysis of SD7037 fixed wing UAV airfoil. *Materials Today: Proceedings*, 47(10):2547–2552, 2021. doi: 10.1016/j.matpr.2021.05.051.

[8] I. Singh. Effect of plain flap over the aerodynamic characteristics of airfoil NACA 66-015. *International Journal of Innovative Science and Research Technology*, 2(6):353–365, 2017.

[9] D. Pracheta, A. Anup, A. Shahriar, and R.B. Saifur. Computational study on effect of flap deflection on NACA 2412 airfoil in subsonic flow. *Applied Mechanics and Materials*, 829:9–14, 2016.doi: 10.4028/www.scientific.net/AMM.829.9.

[10] S. Srivastava and C.V.N. Aditya. Analysis on NACA 2412 airfoil for UAV based on high-lift devices. *International Journal of Engineering Applied Sciences and Technology*, 1(6):13–16, 2016. doi: 10.13140/RG.2.2.35353.95841.

[11] T. Hassan, M.T. Islam, M.M. Rahman, A.R.I. Ali, and A.A. Ziyan. Evaluation of different turbulence models at low reynolds number for the flow over symmetric and cambered airfoils. *Journal of Engineering Advancements*, 3(01):12–22, 2022. doi: 10.38032/jea.2022.01.003.

[12] S.A. Khan, M. Bashir, M.A.A. Baig, and F.A.G.M. Ali. Comparing the effect of different turbulence models on the CFD predictions of NACA0018 airfoil aerodynamics. *CFD Letters*, 12(3):1–10.doi: 10.37934/cfdl.12.3.110.

[13] C. Suvanjumrat. Comparison of turbulence models for flow past NACA0015 airfoil using OpenFOAM. *Engineering Journal*, 21(3):207–221, 2017. doi: 10.4186/ej.2017.21.3.207.

[14] S.M.A. Aftab, A.S. Mohd Rafie, N.A. Razak, and K.A. Ahmad. Turbulence model selection for low Reynolds number flows. *PLoS ONE*, 11(4):e0153755, 2016. doi: 10.1371/journal.pone.0153755.

[15] S. Bogos, A. Dumitrache, and F. Frunzulica; Turbulence models in CFD simulation of low-Reynolds number airfoils flow. *AIP Conference Proceedings*, 1648:500006, 2015. doi: 10.1063/1.4912704.

[16] C.A. Lyon, A.P. Broeren, P. Giguere, A. Gopalarathnam, and M.S. Selig. *Summary of Low-Speed Airfoil Data*. Vol. 3. SoarTech Publications, 1997.

[17] F.R. Menter. Two-equation eddy-viscosity turbulence models for engineering applications.*AIAA Journal*, 32(8):1598-1605, 1994. doi: 10.2514/3.12149.

[18] H.K. Versteeg and W. Malalasekera. *An Introduction to Computational Fluid Dynamics: The Finite Volume Method*. Pearson Education, 2007.